The current issue and full text archive of this journal is available at
www.emeraldinsight.com/0961-5539.htm

Numerical study of turbulent channel flow with strong temperature gradients

Bamdad Lessani and Miltiadis V. Papalexandris
Département de Mécanique, Université Catholique de Louvain, Louvain-la-Neuve, Belgium

Received 28 November 2006
Revised 30 April 2007
Accepted 30 April 2007

Abstract

Purpose – This paper sets out to perform a detailed numerical study of turbulent channel flow with strong temperature gradients using large-eddy simulations.

Design/methodology/approach – A recently developed time-accurate algorithm based on a predictor-corrector time integration scheme is used in the simulations. Spatial discretization is performed on a collocated grid system using a flux interpolation technique. This interpolation technique avoids the pressure odd-even decoupling problem that is typically encountered in collocated grids. The eddy viscosity is calculated with the extension of the dynamic Smagorinsky model to variable-density flows.

Findings – The mean velocity profile at the cold side deviates from the classical isothermal logarithmic law of the wall. Nonetheless, at the hot side, there is a better agreement between the present results and the isothermal law of the wall. Further, the numerical study predicts that the turbulence kinetic energy near the cold wall is higher than near the hot one. In other words heat addition tends to laminarize the channel flow. The temperature fluctuations were also higher in the vicinity of the cold wall, even though the peak of these fluctuations occurs at the side of the hot wall.

Practical implications – The findings of the paper have applications in the design and analysis of convective heat transfer equipment such as heat exchangers and cooling systems of nuclear reactors.

Originality/value – The paper presents the first numerical results for non-isothermal turbulent channel flow with high wall-temperature ratios (up to 9). These findings can be of interest to scientists carrying out research in turbulent flows.

Keywords Flow, Simulation, Temperature distribution

Paper type Research paper

1. Introduction

In this paper, we present large-eddy simulations (LES) results of incompressible, variable density, turbulent channel flows in the presence of strong temperature gradients. Detailed information about the near wall behaviour of these flows can be obtained via either LES or DNS. Historically, large-eddy simulations of turbulent, wall-bounded flows were first performed in isothermal, incompressible systems. Subsequently, compressible (non-zero Mach number) channel flows were studied via LES; see, for example, Hartel *et al.* (1994), Lenormand *et al.* (2000), Terracol *et al.* (2000), Okong'o *et al.* (2000) and von Kaenel *et al.* (2002) and references therein. Such simulations require the use of fully compressible Navier-Stokes solvers.

However, as the Mach number approaches zero, the governing equations become very stiff and, therefore, the compressible solvers become prohibitively slow. Special numerical techniques such as preconditioning can only partly remove the numerical complexities arising from the stiffness of the governing equations. An alternative way to the numerical

International Journal of Numerical Methods for Heat & Fluid Flow
Vol. 18 No. 3/4, 2008
pp. 545-556

0961-5539
DOI 10.1108/09615530810853727

treatment of low Mach number flows is to employ the so-called low Mach number approximation, Majda and Sethian (1985). However, until recently, there has not been developed an algorithm for these equations that is robust enough to treat flows with strong temperature gradients. As a result, only a few LES studies of low Mach number flows with heat transfer have appeared in the literature. see, for example, Wang and Pletcher (1996), Nicoud (2000), Vazquez and Metais (2002), Dalley *et al.* (2003) and Xu *et al.* (2004).

In particular, and to the authors' best knowledge, large-eddy simulations of channel flows with high-heat transfer rates at low-Mach numbers have only been presented in Wang and Pletcher (1996), Nicoud (2000) and Dalley *et al.* (2003). In Wang and Pletcher (1996) the authors examined wall-temperature ratios of 1.02 and 3, using a fully compressible solver combined with preconditioning. In Nicoud (2000) an incompressible low-Mach number solver was used for flows with wall temperature ratios up to four. Finally, in Dalley *et al.* (2003) the authors presented LES results for flows where the wall heat fluxes were constant (instead of the wall temperatures) using a compressible solver. In that study, the heat flux resulted to wall-to-bulk temperature ratios of 1.5 for the heated case and 0.56 for the cooled case.

In the present study, we focus our attention on channel flows at high wall-temperature ratios in the absence of compressibility effects. Thus, we employ the low-Mach number approximation for the balance equations of mass, momentum and energy. According to this approximation, density variations are due only to temperature variations and not due to pressure variations. Thus, for a perfect gas, the density is inversely proportional to the temperature and is independent of the pressure. LES on these flows are performed with a newly-developed solver for the low-Mach number equations (Lessani and Papalexandris, 2006). This solver is robust enough to treat flows of wall-temperature ratios up to nine. Such ratios are much higher than the ratios considered in the literature thus far.

Large temperature gradients strongly effect the thermo-physical properties of the fluid such as the density, dynamic viscosity and thermal conductivity. As a result of the property variations of the fluid, the near-wall behaviour of the non-isothermal channel flow is substantially different from that of the isothermal one. It is shown that the velocity and temperature fluctuations are considerably weaker in the hot wall region than in the cold wall region. This can be attributed to the increase of the dynamic viscosity with the temperature.

The paper is organized as follows. The governing equations along with a brief description of the algorithm are presented in Section 2. Detailed LES results (including turbulence statistics) for the flows of interest are presented in Section 3. This section also contains a discussion of the effects of heat addition on the mean flow. Finally, Section 4 contains some general remarks about the results that we present herein.

2. Governing equations and numerical method

In LES one computes the motion of the large-scale structures and models the nonlinear interactions between the large-scale structures and the small-scale ones. The governing equations for the large-scales are obtained after filtering. The filtering operation can be written in terms of the convolution integral:

$$\bar{f}(x) = \int_D G(x - x')f(x')\mathrm{d}x'. \tag{1}$$

In the above equation, f is a turbulent field, G is some spatial filter of width equal to the grid spacing, and D is the flow domain. For variable density flows the Favre averaging is used rather than the standard one. A Favre-filtered variable is defined as, $\tilde{\phi} = \overline{\rho\phi}/\bar{\rho}$. After filtering, the equations are non-dimensionalized and the low-Mach number approximation (Majda and Sethian, 1985) is applied to them. This approximation amount to a series expansion of the flow variables with respect to the Mach number. These expansions are substituted into the conservation equations for the mass, momentum, energy, and also into the ideal gas law. Subsequently, by collecting the lowest order terms, the following low-Mach number approximation equations are obtained:

$$\frac{\partial \bar{\rho}}{\partial t} + \frac{\partial \bar{\rho}\tilde{u}_i}{\partial x_i} = 0, \tag{2}$$

$$\frac{\partial \bar{\rho}\tilde{u}_i}{\partial t} + \frac{\partial \bar{\rho}\tilde{u}_i\tilde{u}_j}{\partial x_j} = -\frac{\partial \bar{p}}{\partial x_i} + \frac{1}{Re}\,\frac{\partial}{\partial x_j}\left[(\mu + \mu_t)\left(2\tilde{S}_{ij} - \frac{2}{3}\tilde{S}_{kk}\delta_{ij}\right)\right], \tag{3}$$

$$\bar{\rho}c_p\frac{\partial \tilde{T}}{\partial t} + \bar{\rho}c_p\tilde{u}_j\frac{\partial \tilde{T}}{\partial x_j} = \frac{1}{Re\,Pr}\,\frac{\partial}{\partial x_j}\left[(\kappa + \kappa_t)\frac{\partial \tilde{T}}{\partial x_j}\right] + \frac{\gamma - 1}{\gamma}\,\frac{\mathrm{d}P_0}{\mathrm{d}t}, \tag{4}$$

$$P_0 = \bar{\rho}\tilde{T}. \tag{5}$$

In the equations above, P_0 is the first-order component of the pressure expansion. P_0 is uniform and is interpreted as the thermodynamic pressure. Also, $\bar{p}$ is the second-order component of the expansion. This component is non-uniform and is interpreted as the dynamic pressure. In an open system, P_0 equals the outflow pressure, whereas in closed domains it is calculated via integration of the ideal gas equation of state (5) over the flow domain:

$$P_0 = \frac{M_0}{\int(1/\tilde{T})\mathrm{d}V}, \tag{6}$$

where M_0 is the fluid mass inside the closed domain.

Also, in equation (3), $\tilde{S}_{ij} = 1/2(\partial\tilde{u}_i/\partial x_j + \partial\tilde{u}_j/\partial x_i)$ is the large-scale stress-rate tensor. Given the reference values of density ρ_r, velocity u_r, length L_r, dynamic viscosity μ_r, specific heat $c_{p,\mathrm{r}}$, and thermal conductivity κ_r, the Reynolds and Prandtl numbers may be defined as, $Re = (\rho_\mathrm{r}u_\mathrm{r}L_\mathrm{r})/\mu_\mathrm{r}$ and $Pr = (\mu_\mathrm{r}c_{p,\mathrm{r}})/\kappa_\mathrm{r}$, respectively. A simplified Sutherland law is used for the dimensionless thermal conductivity κ, and dynamic viscosity μ, i.e. $\mu = \kappa = \tilde{T}^{0.7}$ The eddy viscosity μ_t, is calculated with the dynamic Smagorinsky model (Moin *et al.*, 1991; Lilly, 1992). The turbulent heat flux is modeled with a gradient transport model (Moin *et al.*, 1991), with $\kappa_t = \mu_t c_{p,\mathrm{r}}/Pr_t$. The turbulent Prandtl number is set equal to $Pr_t = 0.9$. The ratio of specific heats at the reference temperature is denoted by $\gamma = 1.4$.

The numerical procedure is described in detail in Lessani and Papalexandris (2006). Herein we limit ourselves to a summary of the method. The governing equations are discretized on a collocated grid system, combined with a flux interpolation technique to avoid the pressure odd-even decoupling that is typically encountered when using such grids. This technique was originally applied to

incompressible flows (Rhie and Chow, 1983; Morinishi *et al.*, 1998), and has been generalized to variable density flows in Lessani and Papalexandris (2006).

The discretization of the convective term is achieved via the introduction of three auxiliary scalar fluxes $F_i \equiv \rho u_i$, which are staggered with respect to other variables in space. This implies that each auxiliary flux F_i is defined on the center of the cell interface that is normal to the x_i direction, whereas all flow quantities are evaluated at the centers of the computational cells. The convective terms in the streamwise and spanwise directions are discretized with a fourth-order scheme, whereas the convective terms in the normal direction and all viscous terms are second order. In order to increase the stability of the calculations and the allowable time step, the diffusion terms in the normal direction, where the grid is clustered near the walls, are treated implicitly.

The time integration of the energy equation and the update of the density are performed with a two-stage predictor-corrector scheme. At each stage of this scheme, an Adams-Bashforth method is used for the (time) integration of the momentum equations. The velocity field is calculated with a projection method which results to a Poisson equation for the dynamic pressure. This equation is solved with a Fast Fourier Transform in the periodic directions combined with a tridiagonal solver in the normal direction. For the subgrid-scale model, we have employed the extension of the dynamic Smagorinsky model for variable-density flows (Moin *et al.*, 1991), combined with the least square technique (Lilly, 1992), and with averaging in the periodic directions.

3. Numerical results

In this section, we present the numerical results of the channel flow simulations. First, in order to assess the accuracy of the numerical method, an LES of isothermal channel flow is presented and the results are compared with the existing data in the literature. Subsequently, the LES of non-isothermal channel flow with strong temperature gradients is considered and the effects of heat transfer on the mean flow and the turbulent statistics are discussed.

3.1 Isothermal flow

Let x, y, and z, denote the streamwise, normal, and spanwise directions, respectively. The channel consists of two walls that are parallel to each other and parallel to the xz plane. The dimensions of the domain are $4\pi\delta \times 2\delta \times (4/3)\pi\delta$, with δ being the channel half-width. The boundaries of the domain normal to the x and z directions are periodic. No-slip boundary conditions are assumed on the walls of the channel. The coordinates are normalized according to:

$$x^+ = \rho_w u_\tau x/\mu_w, \quad y^+ = \rho_w u_\tau y/\mu_w, \quad z^+ = \rho_w u_\tau z/\mu_w, \tag{7}$$

with $u_\tau = (\tau_w/\rho)^{1/2}$ being the friction velocity and τ_w being the wall shear stress.

A mesh of 128^3 points is used for the isothermal DNS calculation. Uniform meshes are used in the streamwise and spanwise directions, with $\Delta x^+ \simeq 17.6$ and $\Delta z^+ \simeq 5.9$ (in wall units). A non-uniform mesh with hyperbolic tangent distribution is used in the normal direction. The first mesh point away from the wall is at $y^+_{fp} \simeq 0.23$ and the maximum spacing at the centerline of the channel is $\Delta y^+_{max} \simeq 6.84$. The Reynolds number based on the friction velocity and the channel half width is $Re_\tau = \rho u_\tau \delta/\mu = 180$. The mean velocity profile and the turbulence statistics are shown in Figures 1 and 2.

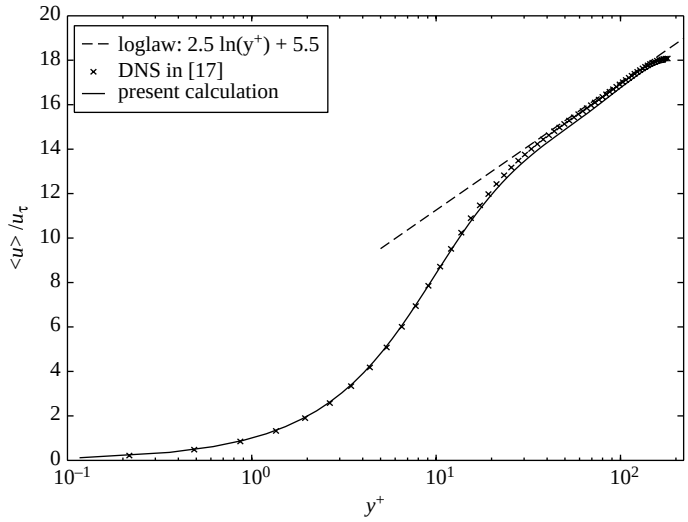

Note: Mean streamwise velocity profile $< u > /u_\tau$ in wall coordinates $y^+ = \rho u_\tau y/\mu$ compared with the DNS in Kim *et al*. (1987)

Figure 1.
Isothermal channel flow

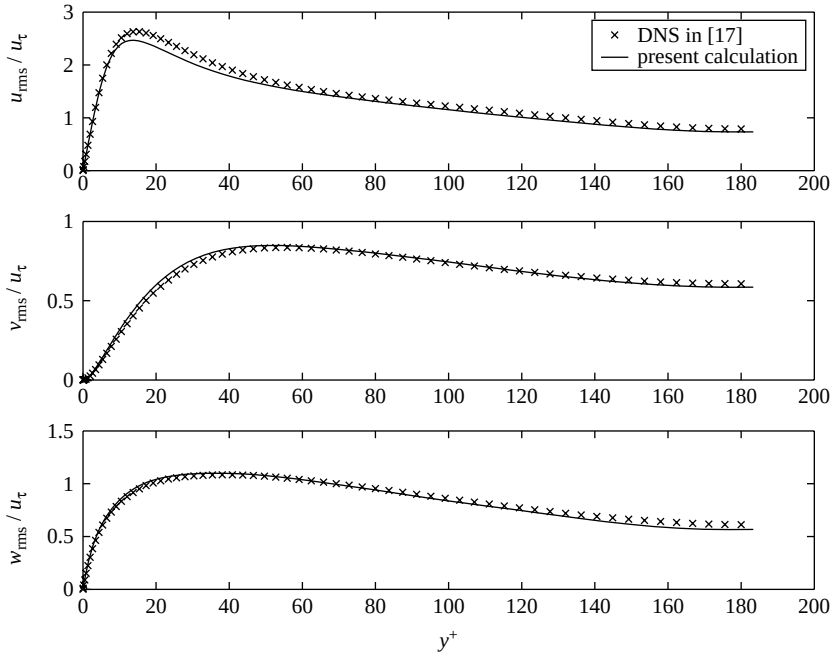

Note: Turbulence intensity (u_{rms}/u_τ, υ_{rms}/u_τ, w_{rms}/u_τ) distributions in wall coordinates $y^+ = \rho u_\tau y/\mu$ for the channel compared with the DNS in Kim *et al*. (1987)

Figure 2.
Isothermal channel flow

From these figures, it can be confirmed that our LES results compare very well with the DNS results in Kim *et al.* (1987).

3.2 Non-isothermal flow

For the non-isothermal turbulent channel flow, we consider a channel whose dimensions are the same as above but the two walls are kept at different temperatures. A mesh of 64^3 points is used for the LES. Uniform meshes are used in the streamwise and spanwise directions. A non-uniform mesh with hyperbolic tangent distribution is used in the wall-normal direction. Let T_h, and T_c denote the temperatures of the hot and cold walls, respectively. Two different cases, corresponding to different wall temperature ratios, are considered herein. More specifically, we have considered ratios of $T_h/T_c = 6$ and 9.

The simulation parameters are listed in Table I. Subscripts "h" and "c" denote the hot and cold wall, respectively. The subscript "w" is used for the values at the walls, $w = \{h, c\}$. The Reynolds number based on the values on the centerline is, $Re_{cl} = \rho_{cl} u_{cl} \delta / \mu_{cl}$. The Reynolds number based on the values near the wall is, $Re_\tau = \rho_w u_{\tau w} \delta / \mu_w$. The friction velocity is $u_{\tau w} = (\tau_w / \rho_w)^{1/2}$, where τ_w is the wall shear stress and ρ_w is the density of the flow in the vicinity of the wall. The average friction velocity is $\bar{u}_\tau = (1/2)(u_{\tau h} + u_{\tau c})$. Finally, the heat flux parameter is defined as $B_{qw} = q_w/(\rho_w c_p u_{\tau w} T_w)$, with q_w the heat flux, and c_p the specific heat at constant pressure.

The flow is driven by the same mean pressure gradient for the two temperature ratios. As a result, by increasing the temperature ratio, the centerline Reynolds number decreases. In particular, $Re_{cl} = 1{,}531$ at $T_h/T_c = 6$, and $Re_{cl} = 1{,}055$ at $T_h/T_c = 9$. The pressure gradient that was considered in our study leads to a centerline Reynolds number of 3,300 when the temperature ratio is equal to 1. The difference between the friction Reynolds numbers of the two walls increases with the temperature ratio. Thus, in order to have a well resolved flow near the wall, one has to pay attention to ensure that the distance of the first grid point (fp), away from the wall satisfies:

$$y^+_{fp} \equiv \frac{\rho_w u_{\tau w} y_{fp}}{\mu_w} < 1.$$

In our calculations this condition has always been satisfied.

In principle, the turbulent Prandtl number can be calculated using the dynamic procedure. During our numerical experiments, however, it was predicted that it remained almost constant from wall to wall for the cases we considered. Therefore, it was subsequently set to a constant value of $Pr_t = 0.9$ for the sake of computational savings. As in earlier LES studies of non-isothermal channel flows (Wang and Pletcher, 1996; Nicoud, 2000), buoyancy forces are neglected. LES studies that take into account these forces, combined with an efficient subgrid-scale model for the mixed effects of property variations and buoyancy, certainly represent an interesting subject. Such studies, however, are beyond the scope of the present article. The mean streamwise velocity profiles $< u^+_{VD} > / u_{\tau w}$ for the hot and cold walls are shown in Figure 3 as

Table I. Simulation parameters for the non-isothermal channel flow

T_h/T_c	Re_{cl}	$Re_{\tau h}$-$Re_{\tau c}$	$u_{\tau h}/\bar{u}_\tau - u_{\tau c}/\bar{u}_\tau$	B_{qh}	B_{qc}
6.0	1,531	32.5-325	1.33-0.64	2.55×10^{-2}	5.60×10^{-2}
9.0	1,055	24.9-376.7	1.42-0.53	2.81×10^{-2}	8.16×10^{-2}

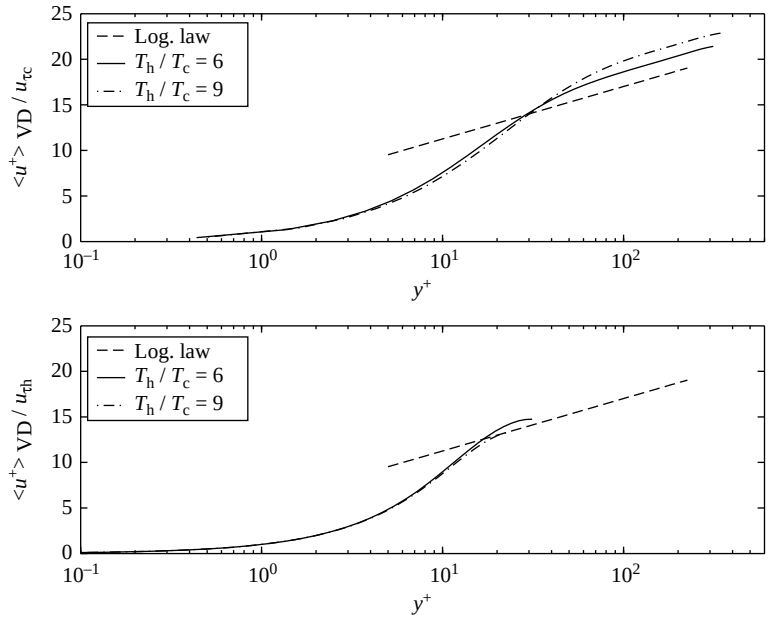

Note: Mean velocity profiles $< u^+_{VD} > / u_{\tau w}$ for the cold (top) and hot (bottom) wall regions in wall coordinates $y^+ = \rho_w u_{\tau w} y / \mu_w$ at two different temperature ratios, T_h/T_c = (6 and 9)

Figure 3.
Non-isothermal channel flow

functions of the wall coordinates $y^+ = \rho_w u_{\tau w} y / \mu_w$. In Figure 3, the logarithmic law of the wall, $u^+ = 2.5 ln y^+ + 5.5$, is also plotted to show the deviation from the isothermal case. In these figures, the van Driest velocity transformation was employed to collapse the results of a variable-density flow into the classical logarithmic law. This transformation is expressed as:

$$u^+_{VD} = \int_0^{u^+} \left(\frac{\rho}{\rho_w}\right)^{1/2} du^+. \tag{8}$$

In Figure 3 (top), at the side of the cold wall, we can observe a significant deviation of the velocity profiles from the reference empirical law of the wall. On the other hand, no such deviation is observed at the side of the hot wall, Figure 3 (bottom). The same over-prediction at the cold wall side was reported in Wang and Pletcher (1996) for a temperature ratio of 3. This deviation may be attributed to the fact that the van Driest transformation does not provide an effective means for collapsing results of variable-density flows if the temperatures (density) variations are too high. On the other hand, the result reported in Nicoud (2000) for a temperature ratio of 4 showed good agreement with the logarithmic law by use of the van Driest transformation. In Nicoud (2000) however, the dimensionless thermal conductivity and dynamic viscosity were chosen to be proportional to $1/\sqrt{T}$ instead of following Sutherland law. Such dependence of the transport coefficients on the temperature is non-physical.

In Figure 4, we present results of the turbulence kinetic energy, $k_t = 1/2 < u'_i u'_i > / \bar{u}^2_\tau$. In this figure, one can see that the velocity fluctuations in the region near the hot wall

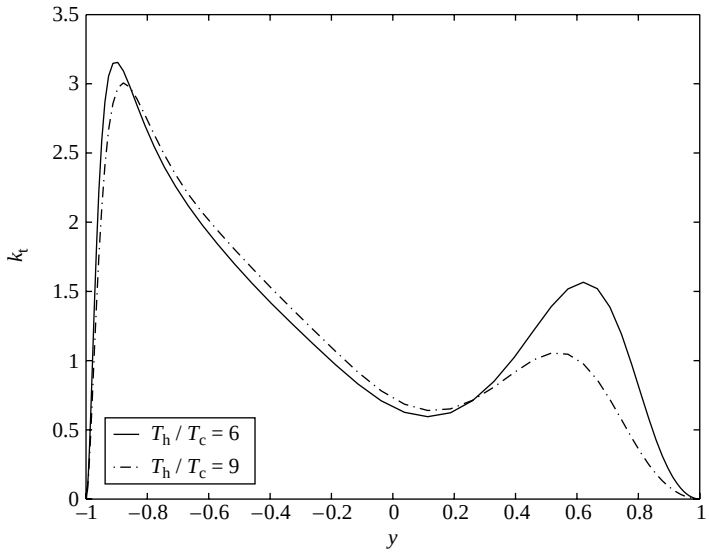

Figure 4.
Non-isothermal channel flow

Note: Turbulence kinetic energy k_t distribution across the channel at two different temperature ratios, $T_h/T_c = 6$ and 9)

decrease and heating tends to laminarize the flow. This can be attributed to the increase of the dynamic viscosity and the decrease of the density in that region. The turbulence intensities ($u_{rms}/\bar{u}_\tau$, $v_{rms}/\bar{u}_\tau$, $w_{rms}/\bar{u}_\tau$) for the cold and hot walls are shown in Figures 5 and 6, respectively, as functions of the wall coordinates $y^+ = \rho_w u_{\tau w} y/\mu_w$. As mentioned before, the subscript "w" is used for the values at the wall, with w = c for the cold wall and w = h for the hot wall. In Figure 5 by comparing the velocity fluctuations at the cold side for the two temperature ratios, it is observed that the magnitudes of the velocity fluctuations in the vicinity of the cold wall are higher for the lower temperature ratio of $T_h/T_c = 6$. Near the core of the channel and away from the cold wall, however, their magnitudes are almost the same. At the hot side in Figure 6, the increase of the temperature ratio seems not to have further effect on the spanwise and normal fluctuations, but it decrease the streamwise component.

Figure 7 (top) shows the mean temperature distribution $(T - T_c)/(T_h - T_c)$, across the channel. We note that the fully developed condition requires that the wall heat flux be the same on both walls. According to the Sutherland law, the thermal conductivity increases with the temperature, which results in a steeper temperature gradient on the cold wall than on the hot wall. In Figure 7 (bottom), the distribution of the temperature turbulent fluctuations T_{rms} is presented. In this figure, we can observe that the temperature fluctuations in the vicinity of the cold wall are higher than the fluctuations in the vicinity of the hot wall. However, the peak of the temperature fluctuations is at the side of the hot wall. And finally, temperature contours at one snapshot at a typical plane normal to the walls are shown in Figure 8. The laminarization of the flow in the vicinity of the hot wall can be clearly seen in these figures for both temperature ratios.

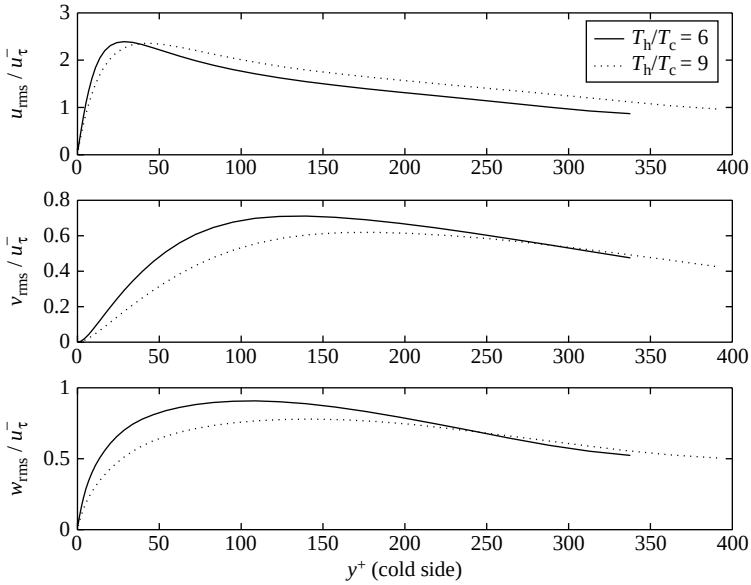

Notes: Turbulence intensities (u_{rms} / u_τ, $\upsilon_{rms} / \bar{u}_\tau$, $w_{rms} / \bar{u}_\tau$) distributions for the cold wall region in wall coordinates $y^+ = \rho_c u_\tau y / \mu_c$ across the channel at two different temperature ratios, $T_h/T_c =$ 6 and 9)

Figure 5.
Non-isothermal channel flow

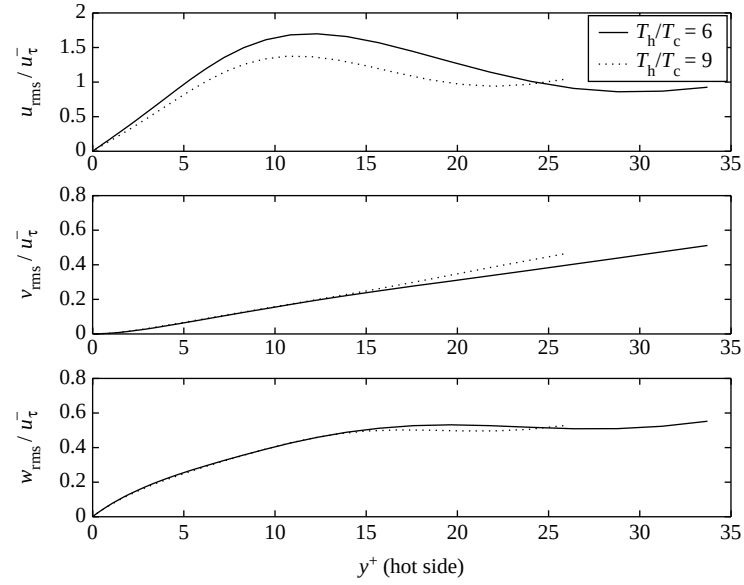

Notes: Turbulence intensities ($u_{rms} / \bar{u}_\tau$, $\upsilon_{rms} / \bar{u}_\tau$, $w_{rms} / \bar{u}_\tau$) distributions for the hot wall region in wall coordinates $y^+ = \rho_h u_{rh} y / \mu_h$ across the channel at two different temperature ratios, T_h/T_c = 6 and 9

Figure 6.
Non-isothermal channel flow

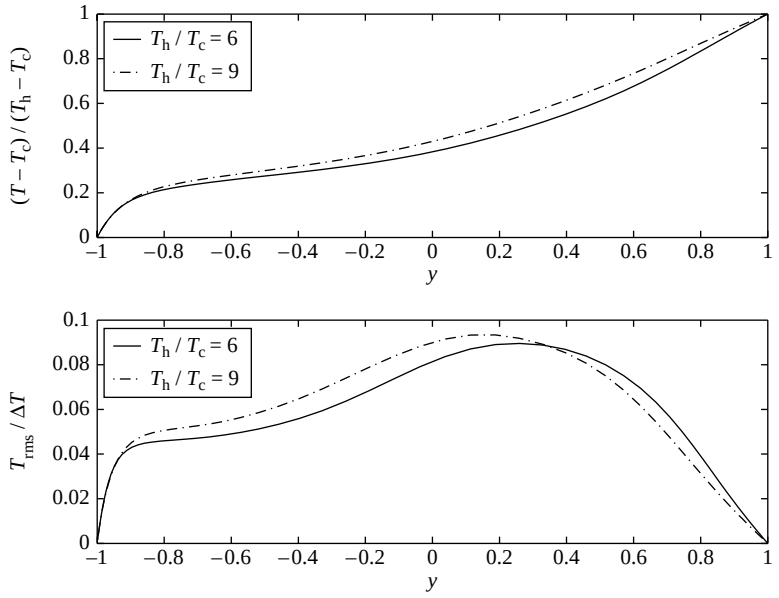

Notes: Top: distribution of mean temperature $(T - T_c)/(T_h - T_c)$ across the channel. Bottom: distribution of temperature turbulent fluctuations T_{rms} across the channel. $T_h/T_c = 6$ and 9)

Figure 7.
Non-isothermal channel flow

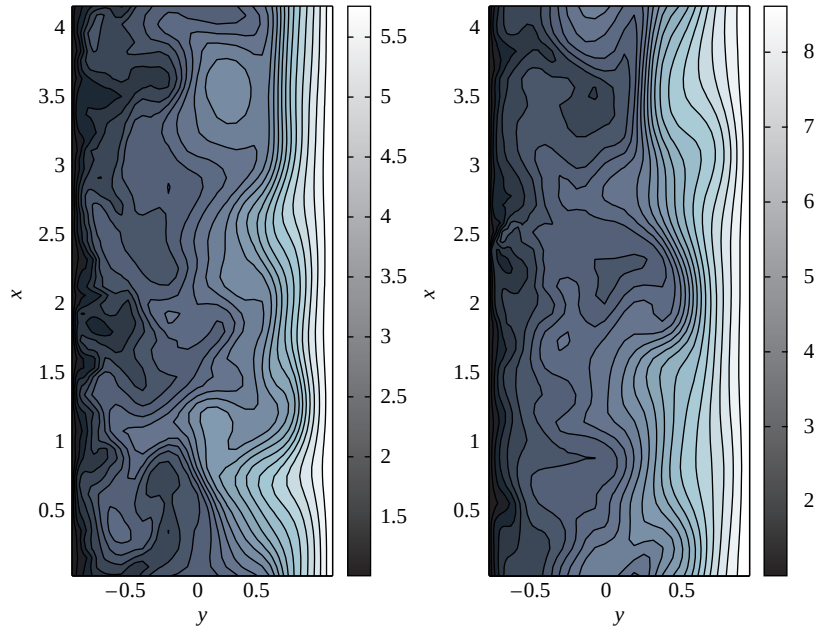

Note: Left: $T_h/T_c = 6$; right: $T_h/T_c = 9$)

Figure 8.
Temperature contours at one snapshot in a typical plane normal to the walls

4. Conclusions

In this paper, an LES study of non-isothermal turbulent channel flows, in particular, flows at low-Mach numbers but with variable thermo-physical properties have been considered. Mean flow quantities as well as turbulent statistics have been presented and discussed. As regards the mean velocities, a van Driest velocity transformation was employed to collapse the results of the variable-density flows considered herein into the classical logarithmic law. It was observed that the mean velocity profile at the cold side deviate from the classical isothermal logarithmic law of the wall. On the other hand, at the hot side, there is a better agreement between the present results and the incompressible isothermal law of the wall. Further, our numerical studies predicted that the turbulence kinetic energy near the cold wall is higher than near the hot one. In other words, heat addition tends to laminarize the channel flow. The temperature fluctuations were also higher in the vicinity of the cold wall, even though the peak of these fluctuations occurs at the side of the hot wall.

References

Dalley, L.D., Meng, N. and Pletcher, R.H. (2003), "Large-eddy simulation of constant heat flux turbulent channel flow with property variations: quasi-developed model and mean flow results", *J. Heat Transfer-Transaction ASME*, Vol. 125 No. 1, pp. 27-38.

Hartel, C., Kleiser, L., Unger, F. and Friedrich, R. (1994), "Subgrid scale energy transfer in the near-wall region of turbulent flows", *Phys. Fluids*, Vol. 6 No. 9, pp. 3130-43.

Kim, J., Moin, P. and Moser, R.D. (1987), "Turbulence statistics in fully developed channel flow at low Reynolds number", *J. Fluid Mech.*, Vol. 177, pp. 133-66.

Lenormand, E., Sagaut, P. and Phuoc, L.T. (2000), "Large-eddy simulation of subsonic and supersonic channel flow at moderate Reynolds number", *Int. J. Num. Meth. Fluids*, Vol. 32 No. 4, pp. 369-406.

Lessani, B. and Papalexandris, M.V. (2006), "Time-accurate calculation of variable-density flows with strong temperature gradients and combustion", *J. Comput. Phys.*, Vol. 212, pp. 218-46.

Lilly, D. (1992), "A proposed modification of the Germano subgrid-scale closure method", *Phys. Fluids A*, Vol. 4, pp. 633-5.

Majda, A. and Sethian, J. (1985), "The derivation and numerical solution of the equations for zero Mach number combustion", *Combustion Science and Technology*, Vol. 42, p. 185.

Moin, P., Squires, K., Cabot, W. and Lee, S. (1991), "A dynamic subgrid-scale model for compressible turbulence and scalar transport", *Phys. Fluids*, Vol. 3, pp. 2746-57.

Morinishi, Y., Lund, T., Vasilyev, O.V and Moin, P. (1998), "Fully conservative higher order finite difference schemes for incompressible flow", *J. Comput. Phys.*, Vol. 143, p. 90.

Nicoud, F. (2000), "Conservative high-order finite difference schemes for low-Mach number flows", *J. Comput. Phys.*, Vol. 158, pp. 71-97.

Okong'o, N., Knight, D.D. and Zhou, G. (2000), "Large-eddy simulations using an unstructured grid compressible Navier-Stokes algorithm", *Int. J. Comp. Fluid Dynamics*, Vol. 13 No. 4, pp. 303-26.

Rhie, C.M. and Chow, W.L. (1983), "A numerical study of the turbulent flow past an airfoil with trailing edge separation", *AIAA J.*, Vol. 21, p. 1525.

Terracol, M., Sagaut, P. and Basdevant, C. (2000), "A multilevel algorithm for large-eddy simulation of turbulent compressible flows", *Comptes Rendus de l'academie des Sciences, Serie II, Fascicule B-Mecanique,Physique, Astronomie*, Vol. 328 No. 1, pp. 81-6.

Vazquez, M.S. and Metais, O. (2002), "Large-eddy simulation of the turbulent flow through a heated square duct", *J. Fluid Mech.*, Vol. 453, pp. 201-38.

von Kaenel, R., Adams, N.A., Kleiser, L. and Vos, J.B. (2002), "The approximate deconvolution model for large-eddy simulation of compressible flows with finite volume schemes", *J. Fluids Eng. Trans. ASME*, Vol. 124 No. 4, pp. 829-35.

Wang, W.P. and Pletcher, R.H. (1996), "On the large-eddy simulation of a turbulent channel flow with significant heat transfer", *Phys. Fluids*, Vol. 8 No. 12, pp. 3354-66.

Xu, X.F., Lee, J.S., Pletcher, R.H., Shehata, A.M. and McEligot, D.M. (2004), "Large-eddy simulation of turbulent forced gas flows in vertical pipes with high heat transfer rates", *Int. J. Heat Mass Transfer*, Vol. 47 Nos 19/20, pp. 4113-23.

Corresponding author
Miltiadis V. Papalexandris can be contacted at: miltos@term.ucl.ac.be